SEMARAK ILMU PUBLISHING

Journal of Advanced Research in Fluid Mechanics and Thermal Sciences

Journal homepage:
https://semarakilmu.com.my/journals/index.php/fluid_mechanics_thermal_sciences/index
ISSN: 2289-7879

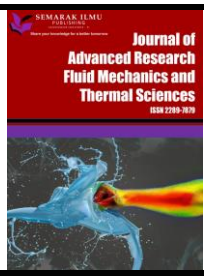

Peristalsis of Fractional Second Grade Fluid in the Presence of Electro Osmotic Phenomenon with Heat and Mass Transfer

Mahadev Madivalappa Channakote[1,*], Dilipkumar Vilasrao Kalse[2], Asha Shivappa Kotnurkar[3], Shekar Marudappa[4]

[1] Department of Mathematics and Statistics, M. S. Ramaiah University of Applied Sciences, Bangalore, India
[2] Department of Mathematics, Guru Nanak Dev Engineering, Bidar, India
[3] Department of Mathematics, Karnataka University, Dharwad, India
[4] Department of Mathematics, B. M. S. College of Engineering, Bangaluru, India

ARTICLE INFO

Article history:
Received 17 October 2023
Received in revised form 16 January 2024
Accepted 30 January 2024
Available online 29 February 2024

Keywords:
EDL; heat and mass transfer; Caputo's fractional derivative; peristaltic flow; second grade fluid

ABSTRACT

MRI method is used in magnetic resonance imaging (MRI) to diagnose brain disorders by detecting the changing conditions within the brain. Peristaltic waves created on the flexible walls of the brain cause particles to move, and understanding this fluid flow can benefit the treatment of malignant tissues. In light of this, the electro-osmotic impact on the peristaltic flow of a fractional second grade fluid (ionic solution) in a microchannel with a heat and mass transfer is investigated. The governing equations of the modulated problem can be solved analytically by assuming a low Reynolds number ($R_e \to 0$) and a long wavelength ($\delta \ll 1$). An analysis of the Poisson-Boltzmann equation is considered to examine the electro-kinetic mechanism. Using the Mathematica program, we solved a set of dimensionless equations and displayed the generated graphs. We analyzed relevant factors for their impacts on temperature, velocity, and pressure gradient. Biomedical engineers may find inspiration to create bio-microfluidic devices that aid in the movement of physiological fluids based on the model and its related findings.

1. Introduction

Muscle contractions create the wave-like motion known as peristalsis, which carries food and liquids. It is an involuntary physical reaction that cannot be consciously regulated by an individual. Smooth muscles involved in peristalsis require a stimulus to contract. Most of the physiological flows are governed by peristaltic activity in a vessel whose main purpose is the biofluid transport. It is generated by the continuous contraction and relaxation of vessels walls. Certain conditions can interfere with peristalsis, a key digestion mechanism. This interference can significantly impact the movement of fluids in various physiological processes, such as blood flow through microscopic blood vessels, the passage of urine from the kidneys to the bladder, and the movement of chyme in the digestive tract. Due to its widespread mechanical and biological applications, peristaltic fluid

* *Corresponding author.*
E-mail address: mchannakote@rediffmail.com

https://doi.org/10.37934/arfmts.114.2.5065

transport has recently gained significant attention. In industrial settings, this type of flow provides an effective method for transporting sanitary fluids. The revolutionary research by Latham [1] and Shapiro *et al.,* [2] on the peristaltic motion of viscous fluids has significantly advanced the literature on different fluids and various geometry regimes under various boundary conditions through experimental, analytical, and numerical advancements. Recent studies in this area can be found in previous researches [3-13].

The issue of electro-osmotic flow regimes has become increasingly important in the field of biomedical engineering and technology. Scientists are particularly interested in studying the interaction between electric fields and fluid particles. Electro-osmotic flow is a particularly useful method for facilitating effective micro-pumping in microchannels. The electric potential in the microchannel affects the Coulomb force, which is responsible for the electro-osmosis process. Bio microfluidics, a key area of study in biomedical engineering and research, focuses on the study of biofluids in micro vessels. The potential use of electrokinetic processes to manipulate and regulate fluid flow in microfossils has garnered significant attention. Microfluidic devices have demonstrated potential in the analysis of biofluids, especially in fluid mixing, species separation, and DNA manipulation, making them valuable tools for studying a variety of biological processes. Additionally, there is a growing interest in the use of mathematical models to study peristaltic transport in microfluidic devices, due to their wide-ranging applications in biomedical engineering. Chakraborty [13] conducted a study on the potential improvement of peristaltic movement through electroosmosis, with a focus on Newtonian fluids. Nevertheless, this model provides a clear method for assessing electro-peristaltic transit. Researchers worldwide have placed significant emphasis on the electro-osmotic process in conjunction with peristalsis in various channels. The significant findings in this order are based on previous studies [14-18].

A bio-mathematical model for electro-osmotic controlled hemodynamic blood flow inside symmetric and non-symmetric arteries with joule heating has been constructed by treating blood as an aqueous solution of Na^{+}, Cl^{-} [19]. Khan *et al.,* [20] elucidated the peristaltic flow of ionic viscoelastic fluid in a curved micro-channel with viscous dissipation, demonstrating the manifestation of electro-osmosis. Additionally, Butt *et al.,* [21] addressed the study of peristaltic streaming flow using thermally conductive electro-osmotic pressure-driven propulsion and a nanomaterial suspended in a micro-ciliated tube.

The study of heat transfer during peristalsis is a fascinating area with numerous potential applications and rapid advancements in the biomedical field. These include oxygenation, haemodialysis, and drug delivery systems. Many researchers are exploring bioheat transfer due to its potential uses in thermotherapy and the human thermoregulation system. Heat transfer is now used to describe the flow of bioheat in the human body. The presence of a chemical reaction in the creation of reservoirs, drying, enhancing oil recovery, flow in desert coolers, insulation, and evaporation at the surface of a water body are all known to be heavily influenced by heat and mass transport. When modeling biological fluids, a comprehensive understanding of fluid dynamics is greatly enhanced by studying the characteristics of heat transfer. Some recent attempts can be found in the previous studies [22-29]. Sinha and Shit [30] examined the exchange of blood temperature through capillaries. Shit *et al.,* [31] demonstrated the EOF for heat transfer and MHD. The wavy walls in electro-kinetic flow are also believed to aid in mass transfer during medical procedures. Hasen and Abdulhadi [32] discussed the Soret and Dufour effect in the analytical study of electro-osmotic peristaltic flow using the Rabinowitsch fluid model. Noreen *et al.,* [33] analyzed peristaltic pumping electroosmotic flow for heat transfer in non-Darcy porous media. Guo and Qi [34] studied the electro-osmotic peristalsis of fractional Jeffrey fluid in an analytical solution in a micro-channel.

Additionally, the non-Newtonian behaviour of the fluid can be described using fractional calculus, a widely recognized model. Substantial advancements have been achieved in studying the viscous properties through fractional calculus, especially with the fractional second-grade model, a viscoelastic fluid model. Converting regular time derivatives to fractional-order time derivatives is a standard method for developing the fractional second-grade model, making it a valuable tool for investigating viscoelastic properties. The peristaltic flow of fractional viscoelastic liquid has recently become significant due to its diverse applications in areas such as life science, physical science, and bioengineering. Recent studies also reported on the second-grade fluid with different geometry [35-41].

To our knowledge, there is no investigations on the peristaltic flow of fractional second-grade fluid with mass and heat transmission under the influence of electro-osmosis. In this work, we discuss some motivating features of flow in the electro-osmotic phenomenon, as well as heat and mass transfer characteristics. Our analysis shows that applying an external electric field can initiate the flow of bio fluids and allow for the analysis of their characteristics. Our main findings indicate that electro-osmosis plays a crucial role in controlling flow and heat transmission. This work may have implications for design, haematology, electrophoresis, and the development of bio-mimetic electro-osmotic pumps, among other fields. The article is structured as follows: Section 1 presents the introduction. Section 2 presents the modelling for equations and relevant boundary conditions in both dimensional and dimensionless variables. Analytical answers are provided in Section 3, while Section 4 presents the key results of the issue. The concluding remarks are presented in the final section.

Caputo's Definition:

The fractional-order derivative according to Caputo's is defined as [36]:

$$D^{\alpha_1} f(t) = \frac{1}{\Gamma(n-\alpha_1)} \int_b^t \frac{f^n(\tau)}{(t-\tau)^{\alpha_1+1-n}}\, d\tau$$

$$Re(\alpha_1) \leq n, n(n-1) \in N,$$

where b is the starting value of the function f and α_1 represents the order of the derivative, which may be real or even complex. For Caputo's derivatives, we have

$$D^{\alpha_1} t^{\beta_1} = \begin{cases} 0 & (\beta_1 \leq \alpha_1 - 1) \\ \frac{\Gamma(\beta_1+1)}{\Gamma(\beta_1-\alpha_1+1)} t^{\alpha_1} & (\beta_1 \geq \alpha_1 - 1). \end{cases}$$

2. Problem Formulation

We have considered the peristaltic propulsion of incompressible viscoelastic fluid in a vertical tube. To analyze the viscoelastic behavior of the fluid, a fractional second-grade fluid model is employed. The cylindrical form $(\tilde{r}, \tilde{x})$ has been chosen so that $\tilde{x}$ is looked at across the tube centerline and $\tilde{r}$ is looked at across the radial tendency of the tube. The peristaltic motion is generated by sinusoidal waves moving along the tube walls at a constant speed, c. The walls of the tube are maintained at constant temperatures T_0 and T_1, respectively. The problem's geometry is illustrated in Figure 1.

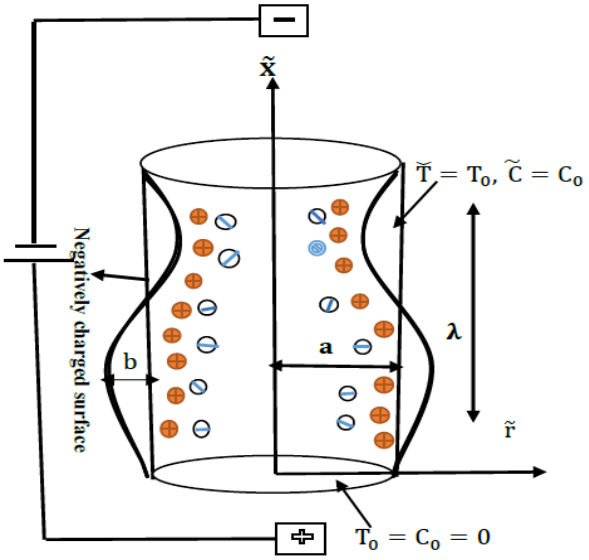

Fig. 1. Diagram of the physical model

The basic equation for viscoelastic fluid with a fractional second-grade model may be found by using the relation given below:

$$\tilde{S} = \mu \left(1 + \tilde{\lambda}_1^{\alpha_1} \frac{\partial^{a_1}}{\partial \tilde{t}^{a_1}}\right) \dot{\gamma}, \tag{1}$$

where $\tilde{S}$ is the shear stress, $\tilde{\lambda}_1$ is the physical constant, $\tilde{t}$ is the time, μ is the viscosity, $\dot{\gamma}$ represents the shear strain rate, and α_1 is the fractional time derivatives such that $(0 < a_1 \leq 1)$. This model is simplified to second grade when $\alpha_1 = 0$ and the conventional Navier-Stokes equation is found by setting $\tilde{\lambda}_1 = 0$.

The conservation of mass, linear momentum, and concentration laws are listed below:

$$\frac{\partial \tilde{u}}{\partial \tilde{x}} + \frac{1}{\tilde{r}} \frac{\partial}{\partial \tilde{r}} (\tilde{v} \tilde{r}) = 0, \tag{2}$$

$$\rho \left(\frac{\partial \tilde{u}}{\partial \tilde{t}} + \tilde{u} \frac{\partial \tilde{u}}{\partial \tilde{x}} + \tilde{v} \frac{\partial \tilde{u}}{\partial \tilde{r}}\right) = -\frac{\partial \tilde{p}}{\partial \tilde{x}} + \mu \left(1 + \tilde{\lambda}_1^{\alpha_1} \frac{\partial^{a_1}}{\partial \tilde{t}^{a_1}}\right) \left[\frac{1}{\tilde{r}} \frac{\partial}{\partial \tilde{r}} \left(\tilde{r} \frac{\partial \tilde{u}}{\partial \tilde{r}}\right) + \frac{\partial^2 \tilde{u}}{\partial \tilde{x}^2}\right] + \rho g a (\tilde{T} - T_0) + \rho g a (\tilde{C} - \check{C}_0) + \rho_e E_x \tag{3}$$

$$\rho \left(\frac{\partial \tilde{v}}{\partial \tilde{t}} + \tilde{u} \frac{\partial \tilde{v}}{\partial \tilde{x}} + \tilde{v} \frac{\partial \tilde{v}}{\partial \tilde{r}}\right) = -\frac{\partial \tilde{p}}{\partial \tilde{r}} + \mu \left(1 + \lambda_1^{\alpha_1} \frac{\partial^{\alpha_1}}{\partial \tilde{t}^{\alpha_1}}\right) \left[\frac{1}{\tilde{r}} \frac{\partial}{\partial \tilde{r}} \left(\tilde{r} \frac{\partial \tilde{v}}{\partial \tilde{r}}\right) + \frac{\partial^2 \tilde{v}}{\partial \tilde{x}^2}\right], \tag{4}$$

$$\rho c_p \left(\frac{\partial \tilde{T}}{\partial \tilde{t}} + \tilde{u} \frac{\partial \tilde{T}}{\partial \tilde{x}} + \tilde{v} \frac{\partial \tilde{T}}{\partial \tilde{r}}\right) = k_1 \left(\frac{\partial^2 \tilde{T}}{\partial \tilde{r}^2} + \frac{1}{\tilde{r}} \frac{\partial \tilde{T}}{\partial \tilde{r}} + \frac{\partial^2 \tilde{T}}{\partial \tilde{x}^2}\right) + Q_0, \tag{5}$$

$$\left(\frac{\partial \tilde{C}}{\partial \tilde{t}} + \tilde{u} \frac{\partial \tilde{c}}{\partial \tilde{x}} + \tilde{v} \frac{\partial \tilde{c}}{\partial \tilde{r}}\right) = D_m \left(\frac{\partial^2 \tilde{C}}{\partial \tilde{r}^2} + \frac{1}{\tilde{r}} \frac{\partial \tilde{C}}{\partial \tilde{r}} + \frac{\partial^2 \tilde{C}}{\partial \tilde{x}^2}\right) + \frac{D_m K_T}{T_m} \left(\frac{\partial^2 \tilde{T}}{\partial \tilde{r}^2} + \frac{1}{\tilde{r}} \frac{\partial \tilde{T}}{\partial \tilde{r}} + \frac{\partial^2 \tilde{T}}{\partial \tilde{x}^2}\right) \tag{6}$$

The total mass remains conserved in the closed system, as stated in Eq. (2). Eq. (3) and Eq. (4) show that the axial (x) and radial (r) components of the system's linear momentum are conserved in the absence of outside influences. Eq. (5) states that an isolated system's total energy remains constant, in accordance with the conservation of energy. Additionally, Eq. (6) expresses Fick's second law of diffusion, which explains how diffusion leads to fluctuations in concentration over time.

The Poisson-Boltzmann equation in electrostatics defines the potential drop scattering for symmetric binary electrolytes in the electrostatics.

$$\nabla^2\Phi = -\frac{\rho_e}{\varepsilon}. \tag{7}$$

The overall charge density is represented by ρ_e, while the permittivity is written as ε. When the Debye-Huckel linearization approach is employed and the ionic concentration is intimate, the microchannel does not fluctuate longitudinally.

$$\rho_e = -\frac{2\, n_0\, z^2 e^2 \Phi}{K_B T_a}, \tag{8}$$

where n_0 denotes the bulk concentration, z is the valency of ions, e denotes the electron charge, K_B is the Boltzmann constant, T_a is the electric solution's mean temperature.

Let's introduce a subsequent dimensionless variable:

$$\left.\begin{array}{c} u = \frac{\tilde{u}}{c}, v = \frac{\tilde{v}}{c\delta}, x = \frac{\tilde{x}}{\lambda}, r = \frac{\tilde{r}}{a}, \delta = \frac{a}{\lambda},\ p = \frac{\tilde{p}a^2}{\mu\, c\, \lambda}, Re = \frac{\rho\, c\, a\, \delta}{\mu}, \\ \theta = \frac{\tilde{T}-T_0}{T_0}, t = \frac{c\tilde{t}}{\lambda}, \phi = \frac{b}{a}, \Theta = \frac{\tilde{C}-C_0}{C_0}, Gr = \frac{\rho g \alpha\, a^2 T_0}{\mu c}, \mathrm{pr} = \frac{c_p \mu}{k}, \\ \mathbf{B} = \frac{\alpha^2 Q_0}{k\, T_0}, \Phi = \frac{\tilde{\Phi}}{\zeta}, Sc = \frac{\mu}{D_m \rho}, Sr = \frac{\rho D_m K_T T_0}{\mu T_m C_0}, Gn = \frac{\rho\, g\, \alpha\, a^2 C_0}{\mu c} \\ h = \frac{\tilde{h}}{a}, \lambda_1 = \frac{c\tilde{\lambda}_1}{\lambda}, S = \frac{\tilde{s}a}{\mu c} \end{array}\right\}, \tag{9}$$

where, Gr is the Grashof number, Gn is the local Grashof number, Sr is the Soret parameter, Sc is the Schmidt number, Pr Prandtl number, $\mathbf{B}$ is the heat source/sink parameter, g is the acceleration due to gravity, T is the temperature, c_p is the specific heat.

Eq. (1) to Eq. (8) take on the resulting form with the aid of Eq. (9) by utilizing the assumption

$(\delta \ll 1)$ and $(R_e \to 0)$,

$$\frac{\partial u}{\partial x} + \frac{1}{r}\frac{\partial}{\partial r}(vr) = 0, \tag{10}$$

$$\frac{\partial^2\Phi}{\partial r^2} + \frac{1}{r}\frac{\partial\Phi}{\partial r} = m^2\Phi, \tag{11}$$

$$\frac{\partial p}{\partial x} = \mu\left(1 + \lambda_1^{\alpha_1}\frac{\partial^{a_1}}{\partial \tilde{t}^{a_1}}\right)\left[\frac{\partial^2 u}{\partial r^2} + \frac{1}{r}\frac{\partial u}{\partial r}\right] + Gr\,\theta + Gn\Theta + m^2\Phi\, U_{hs}, \tag{12}$$

$$\frac{\partial p}{\partial r} = 0, \tag{13}$$

$$\left[\frac{\partial^2\theta}{\partial r^2} + \frac{1}{r}\frac{\partial\theta}{\partial r}\right] + \mathbf{B} = 0, \tag{14}$$

$$\frac{1}{Sc}\left[\frac{\partial^2\Theta}{\partial r^2} + \frac{1}{r}\frac{\partial\Theta}{\partial r}\right] + Sr\left[\frac{\partial^2\theta}{\partial r^2} + \frac{1}{r}\frac{\partial\theta}{\partial r}\right] = 0 \tag{15}$$

where $m = aez\left(\frac{2n_0}{\varepsilon K_B T}\right)^{\frac{1}{2}} = \frac{a}{\lambda_d}$ symbolizes the ratio of the specific transverse length to the Debye-length, λ_d is the Debye -length or EDL, $U_{hS} = -E_x\,\varepsilon\zeta/\mu c$ is extreme electro-osmotic.

The pertinent boundary conditions are:

$$\frac{\partial \Phi}{\partial r} = 0, \text{at } r = 0\,, \Phi = 0 \text{ at } r = h\,, \tag{16}$$

$$\frac{\partial \mathrm{u}}{\partial r} = 0, \text{at } r = 0, \mathrm{u} = 0 \text{ at } r = h\,, \tag{17}$$

$$\frac{\partial \theta}{\partial r} = 0, \text{at } r = 0, \theta = 0 \text{ at } r = h\,, \tag{18}$$

$$\frac{\partial \Theta}{\partial r} = 0, \text{at } r = 0, \Theta = 0 \text{ at } r = h\,, \tag{19}$$

3. Analytical Solution

When we use the resulting boundary conditions from Eq. (16) after solving the accompanying Eq. (11) we arrive at the following solution.

$$\Phi = \frac{I_0(m\,r)}{I_0(m\,h)}, \tag{20}$$

where I_0 is the Bessel function.

When we solve Eq. (14) using the boundary condition (18), we get

$$\theta = \frac{\mathbf{B}}{4}(h^2 - r^2). \tag{21}$$

Using the comparable boundary conditions provided in Eq. (19), solve the subsequent Eq. (15). As a result, by is the precise term for concentration.

$$\Theta = \frac{1}{4}(r^2 - h^2)\mathrm{ScSr}\mathbf{B} \tag{22}$$

By applying the boundary condition (17) and solving Eq. (12) for r, the following values for the axial velocity are obtained:

$$u = \frac{\left(h^2 - r^2\right)\left(-16\frac{\partial p}{\partial x} + (3h^2 - r^2)(\mathrm{Gr} - \mathrm{GnScSr})\mathbf{B}\right) - 64U_{hs} + \frac{64\,I_0(m,r)U_{hS}}{I_0(m,h)}}{64\left(1 + \lambda_1^{\alpha_1}\frac{\partial^{a_1}}{\partial \bar{t}^{a_1}}\right)}. \tag{23}$$

The volume flow rate is generated by the following equation:

$$Q = \int_0^h 2ru\,dr,$$

As an application of Eq. (23) and the above equation yields.

$$Q = \frac{h^2\left(-6h^2p+h^4(\mathrm{Gr}-\mathrm{GnScSr})\mathbf{B}+\frac{48I_2(m\,h)U_{\mathrm{hs}}}{I_0(m,h)}\right)}{48\left(1+\lambda_1^{\alpha_1}\frac{\partial^{a_1}}{\partial t^{a_1}}\right)}. \tag{24}$$

Thus, the wave frame and the laboratory are

$$R = r, U = u - 1, V = v, X = x - 1, Q = \tilde{Q} - h^2. \tag{25}$$

A mathematical expression for the wall's contraction and relaxation is as follows:

$$h = 1 - \phi\cos^2(\pi X). \tag{26}$$

The time-averaged flow rate Q is intended as:

$$\tilde{Q} = q + 1 - \phi - \frac{3\phi^2}{8} = Q + h^2 - 1 - \phi + \frac{3\phi^2}{8}. \tag{27}$$

Eq. (20) obtains the form as a result of Eq. (23).

$$\frac{\partial p}{\partial x} = \frac{-48\left(1+\lambda_1^{\alpha_1}\frac{\partial^{a_1}}{\partial t^{a_1}}\right)\tilde{Q}I_0(mh)+Grh^6BI_0(mh)-Gnh^6ScSr\mathbf{B}\,\mathrm{I}_0(m\,h)+\,48h^2\mathrm{I}_2(m\,h)U_{\mathrm{hs}}}{6h^4I_0(m\,h)}. \tag{28}$$

when $\mathbf{B} \to 0$ and $U_{hS} \to 0$ are utilized, Eq. (23) and Eq. (28) are reduced to the corresponding (Tripathi *et al.,* 2010) results.

Following are the representations for the heat transfer coefficient:

$$Xh = \left[\frac{\partial\theta}{\partial r}\times\frac{\partial r}{\partial x}\right]_{r=h} = \frac{\mathbf{B}\pi\phi\mathrm{h}}{\mathbf{2}}\times\,\sin(2\pi x) \tag{29}$$

The mass transfer coefficients are represented as follows:

$$Xm = \left[\frac{\partial\Theta}{\partial r}\times\frac{\partial r}{\partial x}\right]_{r=h} = \frac{h\pi\phi\mathrm{ScSr}B}{2}\times\sin\,(2\pi x) \tag{30}$$

The pressure rise per wavelength Δp and friction force F_λ are correspondingly given by:

$$\Delta p = \int_0^1 \frac{\partial p}{\partial x}\,dx, \tag{31}$$

$$F_\lambda = \int_0^1 \left(-h^2\,\frac{\partial p}{\partial x}\right)dx. \tag{32}$$

4. Results and Discussion

The primary objective of this paper is to investigate the electro-osmotic flow of a fractional second-grade fluid with heat and mass transfer in a vertical cylindrical tube. The analysis will focus on the complex flow structure, liquid rheology, Helmholtz-Smoluchowski velocity effects, Debye length effects, Soret and Dufour effects. The acquired solutions will be visually discussed in this section, considering various pertinent parameters. Graphs will be used to illustrate the effects of the Debye-Huckel parameter m, the Helmholtz-Smoluchowski velocity U_{hs}, the thermal Grashof number

Gr, the local concentration Grashof number Gn, the heat source/sink parameter $\mathbf{B}$, and the Schmidt number Sc on the profiles of velocity (u), temperature (θ), concentration (Θ), pressure gradient $\left(\frac{dp}{dx}\right)$, and pressure rise Δp.

Figure 2 and Figure 3 describe the behavior of the velocity profile when the Helmholtz-Smoluchowski velocity U_{hs} and Debye-Huckel parameters m are varied. From Figure 2, it is observed that the magnitude of the fluid velocity increases with an increase in U_{hs}. Here it is said that the velocity distribution rises as a result of the swelling influences of factors and reaches its extreme altitude at $r = 0$. Based on Figure 3, m causes an increase in the magnitude of u, indicating that u expands as m increases in the core area of the channel. λ_d is inversely proportional to EDL, as m represents the ratio of the channel height to the Debye length λ_d. Consequently, the central area, $r = 0$, experiences greater fluid flow. Physically, due to the motion of the cation and anions the electro-osmotic flow (EOF) forms in the core region and consequently the axial velocity increases.

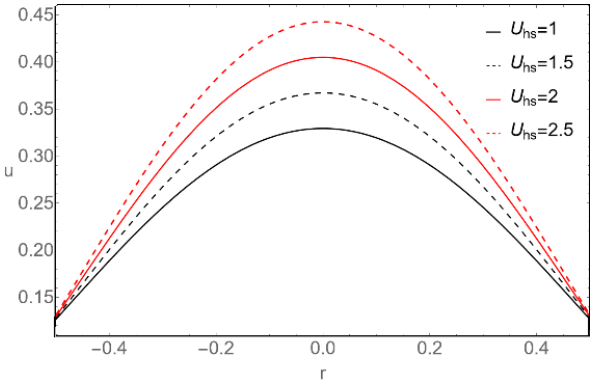

Fig. 2. Change in u for U_{hs},with $\phi = 0.4, x = 0.25, Sr = 3, Sc = 0.4, \mathbf{B} = 4, Q = 0.4, Gn = 1, Gr = 10, t = 0.5, a = 0.2, \lambda_1 = 2$

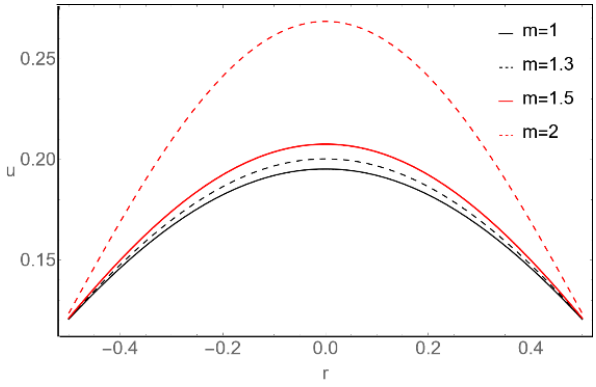

Fig. 3. Change in u for m, with $\phi = 0.2, x = 0.25, Sr = 3, Sc = 0.4, \mathbf{B} = 5, Q = 0.4, Gn = 1, Gr = 10, t = 0.5, a = 0.2, \lambda_1 = 2, U_{hs} = 1$

Figure 4 and Figure 5 illustrate the behavior of the velocity profile for the Soret parameter Sr and the Schmidt number Sc. The figures clearly demonstrate that the extent of the velocity reductions in the middle of the channel differs from its edges. This indicates that as Sc and Sr values increase, the resistive force becomes stronger and directly influences fluid flow. Additionally, from Figure 6, it is evident that velocity increases as the value of the Grashof number Gr rises. Figure 7 illustrates the variance in the velocity profile for different local Grashof numbers, Gn. It is observed that as Gn increases, the velocity decreases in the center of the channel, but the opposite trend is observed near the wall of the channel.

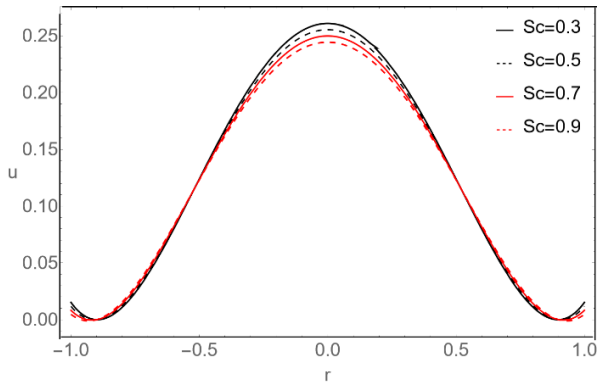

Fig. 4. Change in u for Sc, with $\phi = 0.4, x = 0.25, Sr = 3, \mathbf{B} = 5, \phi = 0.4, Gn = 1, Gr = 10, t = 0.5, a = 0.2, \lambda_1 = 2, U_{hs} = 1$

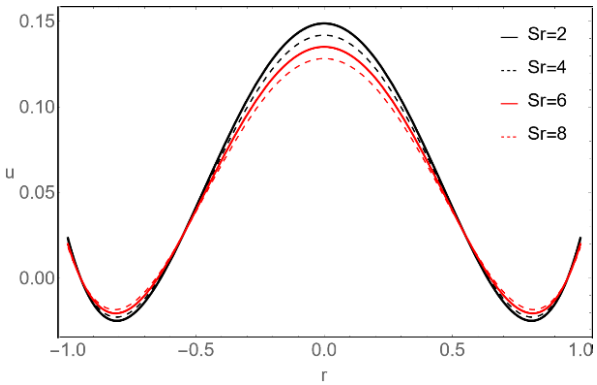

Fig. 5. Change in u for Sr, with $\phi = 0.4, x = 0.25, Sc = 0.4, \mathbf{B} = 4, \phi = 0.4, Gn = 1, Gr = 8, t = 0.5, a = 0.2, \lambda_1 = 1, U_{hs} = 2$

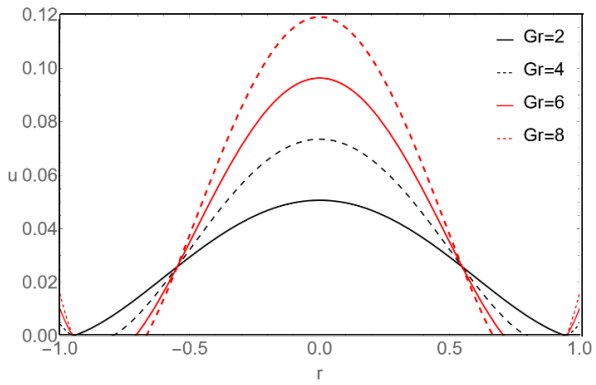

Fig. 6. Change in u for Gr, with $\phi = 0.4, x = 0.25, Sr = 3, Sc = 0.4, \mathbf{B} = 4, \phi = 0.4, Gn = 1, t = 0.5, a = 0.2, \lambda_1 = 2, U_{hs} = 2$

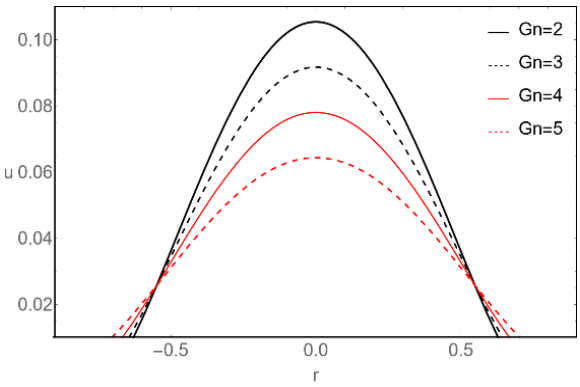

Fig. 7. Change in u for Gn, with $\phi = 0.4, x = 0.25, Sr = 3, Sc = 0.4, B = 4, \phi = 0.4, Gn = 1, Gr = 8, t = 0.5, a = 0.2, \lambda_1 = 1, U_{hs} = 2$

The temperature fluctuation for different values of the source/sink parameter B and amplitude ratio ϕ is analyzed in Figure 8 and Figure 9. In Figure 8, it is observed that the temperature increases with higher values of B. Figure 9 illustrates the temperature variation for the amplitude ratio ϕ, showing that θ decreases as ϕ values increase.

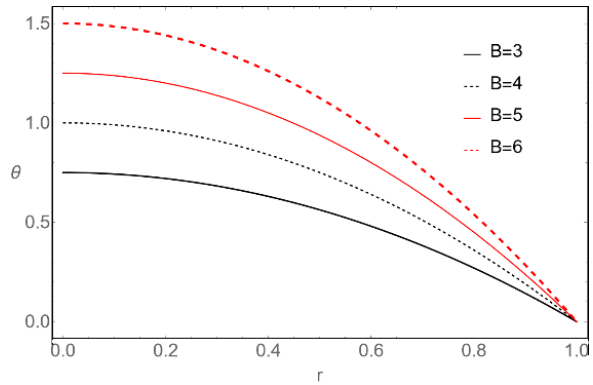

Fig. 8. Effect of **B** on θ

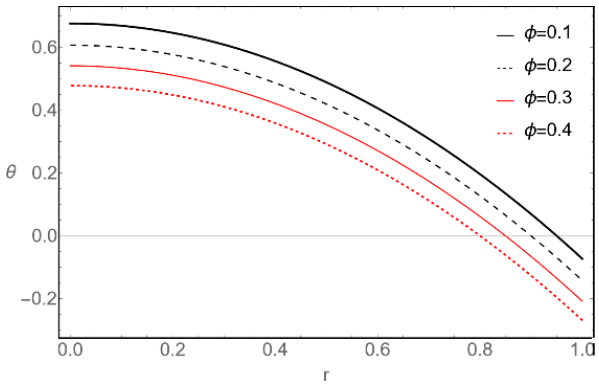

Fig. 9. Effect of ϕ on θ

Figure 10 to Figure 12 depict the assessment of concentration Θ for different Soret number Sr and Schmidt number Sc values. These plots illustrate that as the radial distance r increases, the concentration also increases, but it decreases with higher Soret and Schmidt numbers at the inlet

and downstream. The highest concentration is achieved at the inlet and downstream for various levels of Sr and Sc, respectively. It was determined that the concentration met the boundary criteria.

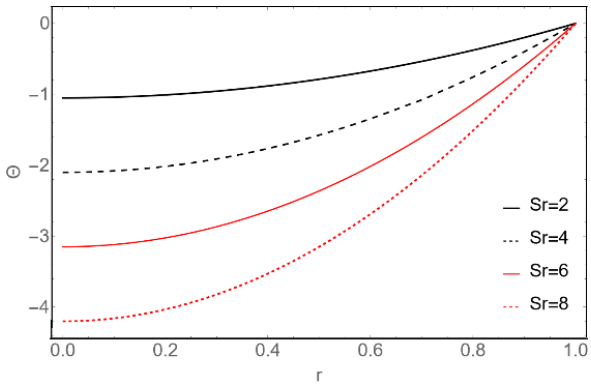

Fig. 10. Effect of Sr on Θ

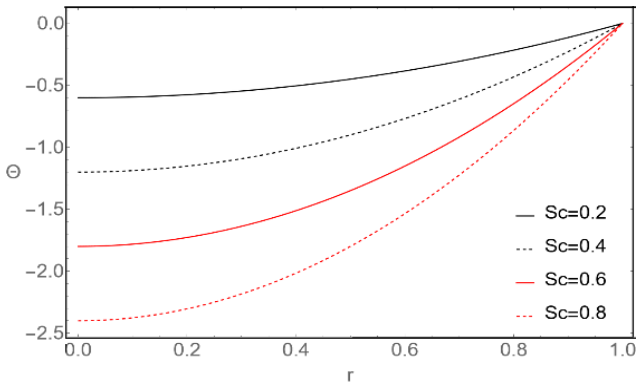

Fig. 11. Effect of Sc on Θ

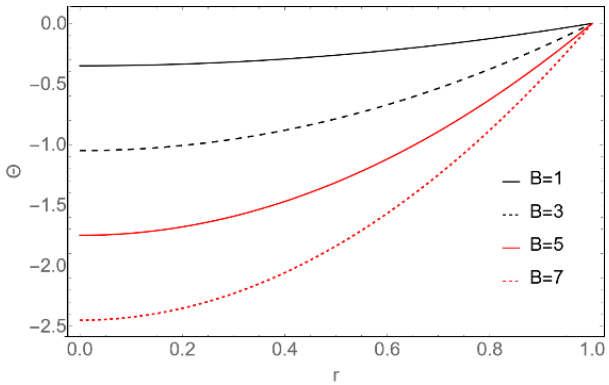

Fig. 12. The concentration Θ vs r for assorted values of **B**, when $\phi = 0.4, x = 0.5, Sr = 2, Sc = 0.2$

Figure 13 to Figure 19 plotted to show the impacts of $U_{hs}, m, Sr, Gn, \mathbf{B}, Sc, \lambda_1$ on $\frac{dp}{dx}$ respectively. It should be noticed that the $\frac{dp}{dx}$ distribution has been depicted in relation to the axial coordinate (x). It is found that the axial length's pressure gradient is sinusoidal in nature, representing high pressure gradients in contraction and low-pressure gradient at relaxation positions, respectively, which creates the peristaltic pumping process. As a result, a controlled volume of liquid can be pumped from one area to another without contaminating it. The pressure gradient along the axial length appears to follow a sinusoidal pattern, with high gradients during contraction and low gradients during relaxation. This pattern initiates the peristaltic pumping process, allowing for regulated and disturbance-free transport of liquid between two locations.

The pressure gradient for Figure 13 shows the pressure gradient for increasing the inverse EDL thickness $(m = a/\lambda_d)$, also known as the Debey-Huckel parameter. It has been observed that the pressure gradient increases as the Debey-Huckel parameter increases. This suggests that a negative pressure gradient may occur when the usual thickness of the EDL reductions. Figure 14 illustrates the relationship between U_{hs} and $\frac{dp}{dx}$. As U_{hs} (Helmotz-Soluchowski velocity) or the external electric field increases, the pressure gradient steadily develops, and a growing external electric field intensity can constrain the negative pressure gradient.

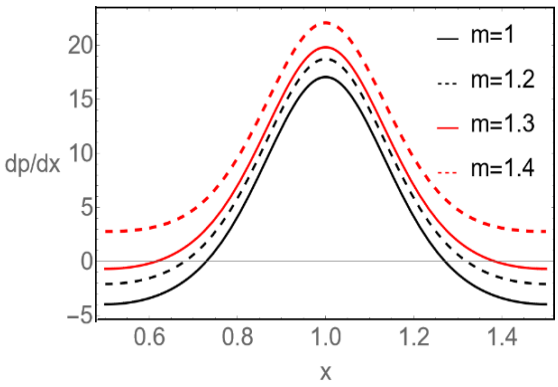

Fig. 13. The pressure gradient $\frac{dp}{dx}$ vs x for distinct values of m, with $\phi = 0.4, x = 0.75, \boldsymbol{\lambda_1} = \mathbf{2}, \mathrm{Sc} = 0.4$

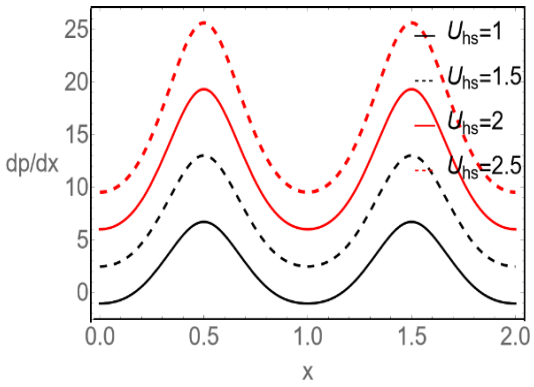

Fig. 14. The pressure gradient $\frac{dp}{dx}$ vs x for distinct values of U_{hs}, with $Gr = 6, \mathbf{B} = 0.3, Sr = 4, Gn = 0.3$

In Figure 15, the impact of the source/sink parameter $\mathbf{B}$ on the pressure gradient is demonstrated. The image reveals that the pressure gradient is small scale for $x \in [0,0.2]$ and $x \in [0.8,1]$, but a significant pressure gradient occurs for $x = [0.5]$. Figure 16 to Figure 19 are portrayed to get the influence of Gn, Sc, Sr *and* λ_1 on the pressure gradient. We clearly see in these figures that pressure gradient diminishes for rising values of local Grashof number, Soret parameter, Schidmit number and material parameter λ_1. Figure 20 and Figure 21 show the pressure rise against the time flow rate Q for diverse values of m, U_{hs}.

The recognized peristaltic passage spectacle is linked to the idea of mathematical pumping. In light of the current investigation, it is therefore justified to look into the pumping region's performance. Figure 20 and Figure 21 show the influence of Debye-Huckel parameter m and Helmholtz-Smoluchowski velocity U_{hs} on the pressure rise Δp. It is prominent from Figure 20 that escalating m, (i.e., reducing the typical extent of the EDL), notably, expands the pressure rise in the region $\Delta p > 0, \Delta p = 0,$ and $\Delta p < 0$. From Figure 21 shows that the pressure increases with increasing Helmholtz-Smoluchowski velocity U_{hs}. Figure 22 and Figure 23 were created to analyse the impact of Soret number Sr and Schmidt number Sc on Δp. The results show that the pressure rise in the pumping region $(\Delta p > 0)$ decreases as Sr and Sc increase.

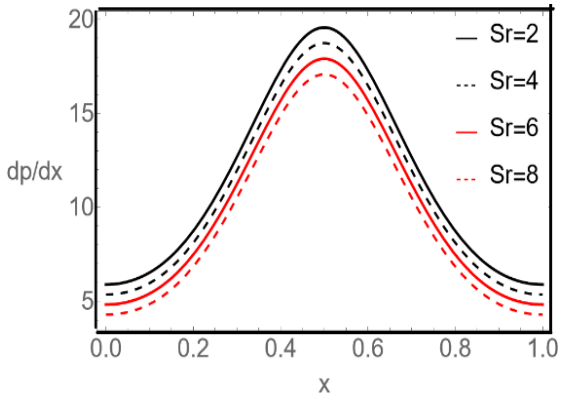

Fig. 15. The pressure gradient $\frac{dp}{dx}$ vs x for distinct values of Sr, with $\phi = 0.4, x = 0.75, \boldsymbol{\lambda_1} = \mathbf{2}, \mathrm{Sc} = 0.4$

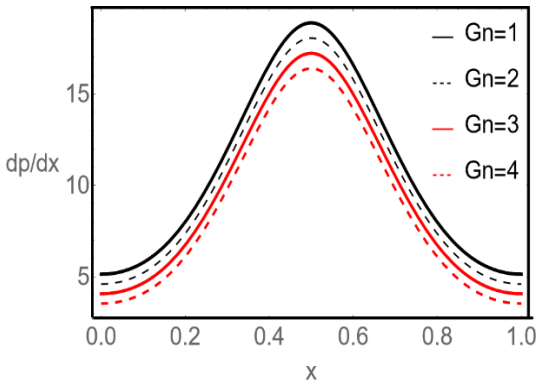

Fig. 16. The pressure gradient $\frac{dp}{dx}$ vs x for distinct values of Gn, with $\mathbf{B} = 0.3, Sr = 4, U_{hs} = 2, Gr = 6$

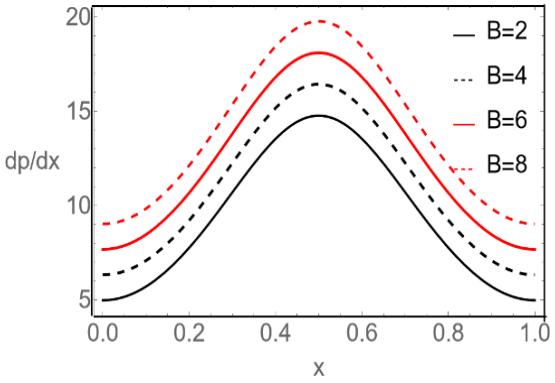

Fig. 17. The pressure gradient $\frac{dp}{dx}$ vs x for multiple values of B, with $Sr = 2, x = 0.5, \mathrm{Gr} = 6, \mathrm{Sc} = 0.2$

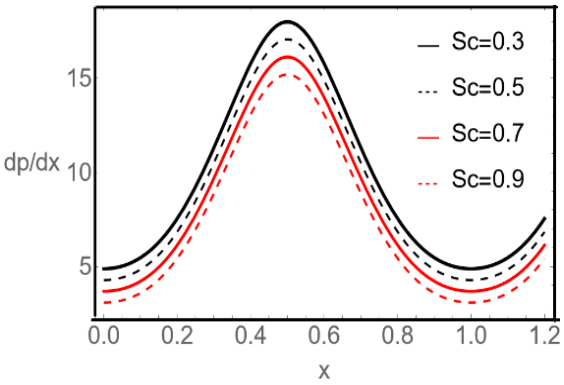

Fig. 18. The pressure gradient $\frac{dp}{dx}$ vs x for multiple values of Sc, with $\mathbf{B} = 0.3$, $Gn = 3, \phi = 0.4, Sr = 2$

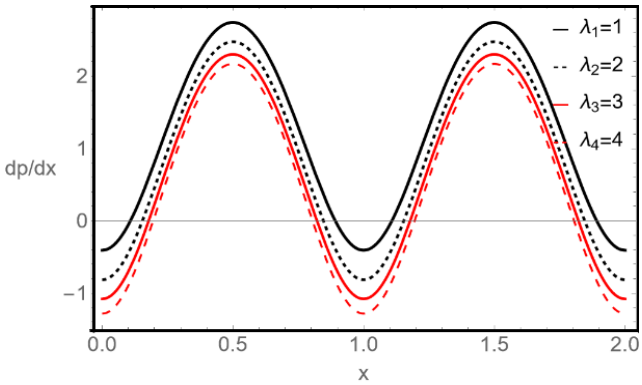

Fig. 19. The pressure gradient $\frac{dp}{dx}$ vs x for multiple values of λ_1 ,with $\phi = 0.4, x = 0.7$ $Sr = 3, Sc = 0.4, B = 4, \phi = 0.4, Gn = 1, Gr = 8, t = 0.5, a = 0.2, U_{hs} = 1, m = 2$

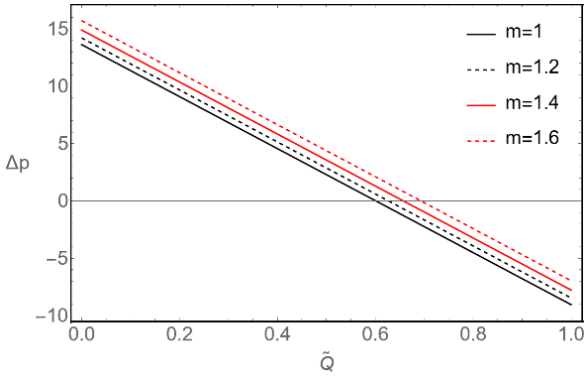

Fig. 20. The pressure rise Δp vs x for multiple values of m, with $\lambda_1 = 2, x = 0.5, \mathrm{Gr} = 6, \mathrm{Sc} = 0.2$

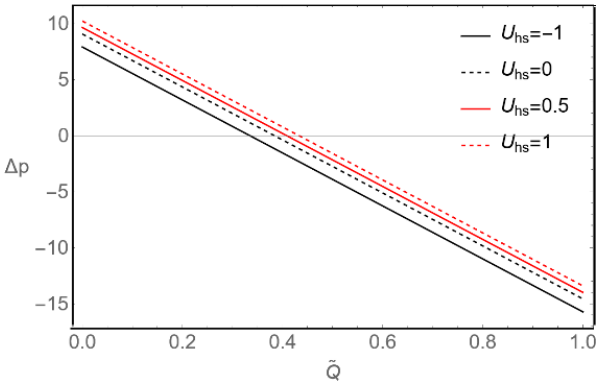

Fig. 21. The pressure rise Δp vs x for multiple values of $U_{hs,}$ with $\mathbf{B} = 0.3$, $Gn = 3, \phi = 0.4, Sr = 2$

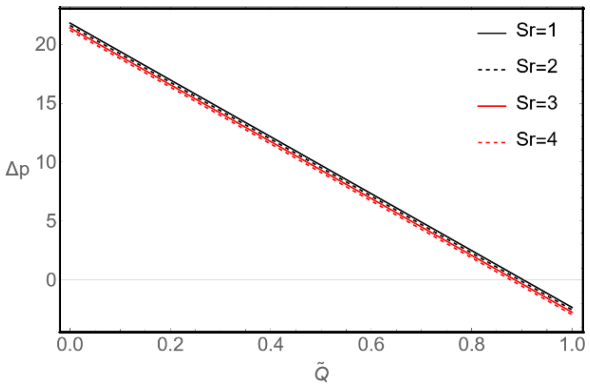

Fig. 22. The pressure rise Δp vs x for multiple values of Sr, with $\lambda_1 = 2, x = 0.5, \mathrm{Gr} = 8, \mathrm{Sc} = 0.2$

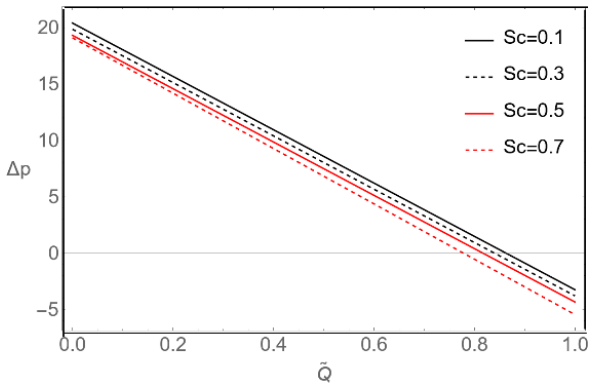

Fig. 23. The pressure rise Δp vs x for multiple values of Sc, with $\mathbf{B} = 0.3$, $Gn = 3, \phi = 0.4, Sr = \mathrm{m} = 1, \mathrm{U_{hs}} = 1$

Temperature gradients contribute to mass fluxes, known as the Soret effect. The Soret effect can be disregarded in the heat and mass transfer mechanism when it is small compared to the effects of Fourier or Fick laws. However, it is significant for isotope separation and the mixing of gases with very light molecular weight (H_2, He) and medium molecular weight (N_2, air), and cannot be ignored. The Schmidt number is a measure of the ratio of momentum diffusivity (kinematic viscosity) to mass diffusivity. It is commonly used to describe fluid flows that involve both momentum and mass diffusion convection processes occurring simultaneously. In heat and mass transfer-related issues, the heat and mass transfer coefficient hold significant physical importance. Therefore, it is beneficial to examine the behaviour of the heat and mass transfer coefficient (Xh and Xm in this case) for the specific problem. In this light, the interaction of heat transfer Xh and mass transfer Xm with various parameters is depicted in Figure 24 to Figure 27. These figures demonstrate the oscillating behavior induced by peristalsis. It is evident from Figure 24 to Figure 27 that the heat and mass transfer coefficient Xh and Xm both increase and decrease with the growth of $B, \phi, Sc, and\ Sr$, respectively.

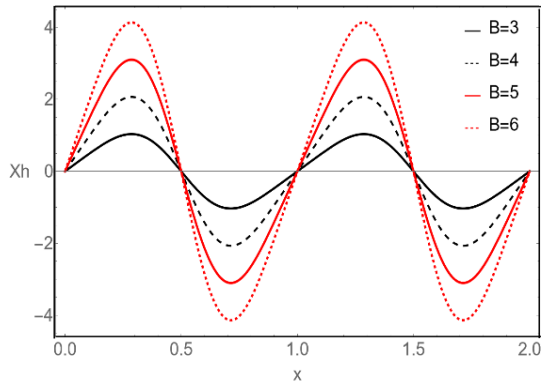

Fig. 24. Influence of B on Xh

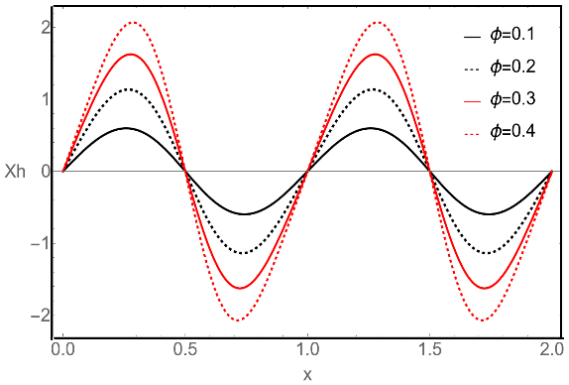

Fig. 25. Influence of ϕ on Xh

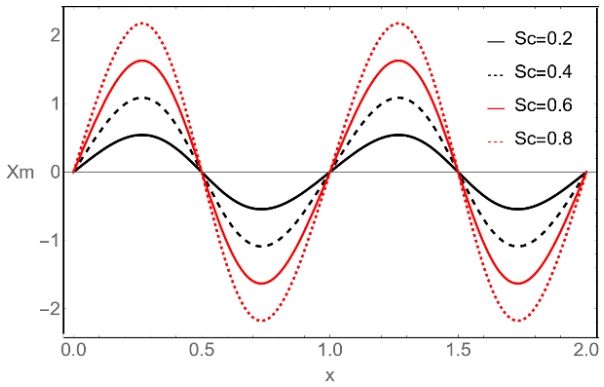

Fig. 26. Influence of Sc on Xm

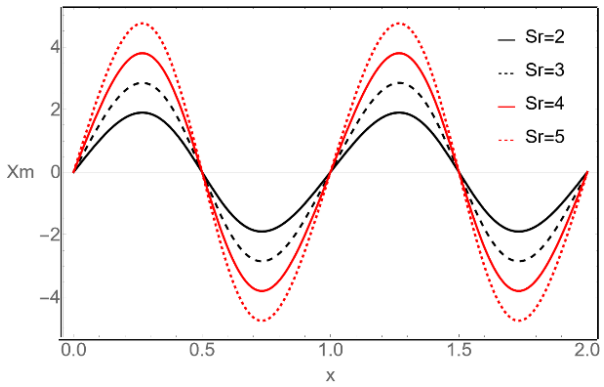

Fig. 27. Influence of Sr on Xm

5. Conclusions

The study examines the effects of heat and mass transfer on the flow of a fractional second-grade fluid model through a cylindrical tube with the EDL phenomenon. The key findings of the study include the observation that as the values of m, $\mathbf{B}$, Gr, and U_{hs} increase, the dimensionless velocity is highest near the center of the tube. The velocity profile is also influenced by the Soret parameter, Schmidt number, and local Grashof number. Additionally, the temperature distribution increases with higher Grashof number Gr and source/sink parameter $\mathbf{B}$, while the concentration field decreases with the Soret parameter Sr and Schmidt number Sc. The pressure gradient and pressure rise are strongly affected by the Debye-Huckel parameter m and Helmholtz-Smoluchowski velocity U_{hs}. Rapid fluctuations in Xh and Xm are observed with changing values of B, ϕ, Sc, and Sr. Therefore, studying the fluid flow of a fractional second-grade fluid under these conditions is beneficial for treating cancerous tissues. Furthermore, the research outcomes can be utilized to develop various types of peristaltic micropumps for transferring rheological fluids in complex systems.

Declarations

Funding

No money, grants, or other forms of upkeep were issued.

Conflicts of Interests

The authors affirm that they have no known financial or interpersonal conflicts that would have seemed to have an impact on the research presented in this study.

Competing Interests

There are no competing interests that the authors can disclose that would affect the article's content.

References

[1] Latham, Thomas Walker. "Fluid motions in a peristaltic pump." *PhD diss., Massachusetts Institute of Technology*, 1966.

[2] Shapiro, Ascher H., Michel Yves Jaffrin, and Steven Louis Weinberg. "Peristaltic pumping with long wavelengths at low Reynolds number." *Journal of Fluid Mechanics* 37, no. 4 (1969): 799-825. https://doi.org/10.1017/S0022112069000899

[3] Rathod, V. P., and M. M. Channakote. "A study of ureteral peristalsis in cylindrical tube through porous medium." *Advances in Applied Science Research* 2, no. 3 (2011): 134-140.

[4] Rathod, V. P., and M. Mahadev. "Effect of thickness of the porous material on the peristaltic pumping of a Jeffry fluidwith non-erodible porous lining wall." *International Journal of Mathematical Archive* 2, no. 10 (2011): 2068-

2077.
[5] Hayat, Tasawar, S. Noreen, N. Ali, and S. Abbasbanday. "Peristaltic motion of Phan-Thien-Tanner fluid in a planar channel." *Numerical Methods for Partial Differential Equations* 28, no. 3 (2012): 737-748. https://doi.org/10.1002/num.20647
[6] Asha, S. K., and G. Sunitha. "Mixed convection peristaltic flow of a Eyring-Powell nanofluid with magnetic field in a non-uniform channel." *JAMS* 2, no. 8 (2018): 332-334. https://doi.org/10.26855/jamc.2018.08.003
[7] Nadeem, S., Arshad Riaz, R. Ellahi, and Noreen Sher Akbar. "Mathematical model for the peristaltic flow of Jeffrey fluid with nanoparticles phenomenon through a rectangular duct." *Applied Nanoscience* 4 (2014): 613-624. https://doi.org/10.1007/s13204-013-0238-5
[8] Mahmood, W., M. Sajid, N. Ali, and M. N. Sadiq. "A new interfacial condition for the peristaltic flow of a micropolar fluid." *Ain Shams Engineering Journal* 13, no. 5 (2022): 101744. https://doi.org/10.1016/j.asej.2022.101744
[9] Sadaf, Hina, and Iqra Shahzadi. "Physiological transport of Rabinowitsch fluid model with convective conditions." *International Communications in Heat and Mass Transfer* 126 (2021): 105365. https://doi.org/10.1016/j.icheatmasstransfer.2021.105365
[10] Ali, Aamir, S. Saleem, Sana Mumraiz, Anber Saleem, M. Awais, and D. N. Khan Marwat. "Investigation on TiO_2-Cu/H_2O hybrid nanofluid with slip conditions in MHD peristaltic flow of Jeffrey material." *Journal of Thermal Analysis and Calorimetry* 143 (2021): 1985-1996. https://doi.org/10.1007/s10973-020-09648-1
[11] Shaheen, A., and S. Nadeem. "Metachronal wave analysis for non-Newtonian fluid under thermophoresis and Brownian motion effects." *Results in Physics* 7 (2017): 2950-2957. https://doi.org/10.1016/j.rinp.2017.08.005
[12] Minerick, Adrienne R., Agnes E. Ostafin, and Hsueh-Chia Chang. "Electrokinetic transport of red blood cells in microcapillaries." *Electrophoresis* 23, no. 14 (2002): 2165-2173. https://doi.org/10.1002/1522-2683(200207)23:14<2165::AID-ELPS2165>3.0.CO;2-#
[13] Chakraborty, Suman. "Augmentation of peristaltic microflows through electro-osmotic mechanisms." *Journal of Physics D: Applied Physics* 39, no. 24 (2006): 5356. https://doi.org/10.1088/0022-3727/39/24/037
[14] Tang, G. H., X. F. Li, Y. L. He, and W. Q. Tao. "Electroosmotic flow of non-Newtonian fluid in microchannels." *Journal of Non-Newtonian Fluid Mechanics* 157, no. 1-2 (2009): 133-137. https://doi.org/10.1016/j.jnnfm.2008.11.002
[15] Bandopadhyay, Aditya, Dharmendra Tripathi, and Suman Chakraborty. "Electroosmosis-modulated peristaltic transport in microfluidic channels." *Physics of Fluids* 28, no. 5 (2016). https://doi.org/10.1063/1.4947115
[16] Tripathi, Dharmendra, Ravindra Jhorar, O. Anwar Bég, and Sachin Shaw. "Electroosmosis modulated peristaltic biorheological flow through an asymmetric microchannel: mathematical model." *Meccanica* 53 (2018): 2079-2090. https://doi.org/10.1007/s11012-017-0795-x
[17] Narla, V. K., and Dharmendra Tripathi. "Electroosmosis modulated transient blood flow in curved microvessels: study of a mathematical model." *Microvascular Research* 123 (2019): 25-34. https://doi.org/10.1016/j.mvr.2018.11.012
[18] Prakash, J., and Dharmendra Tripathi. "Study of EDL phenomenon in Peristaltic pumping of a Phan-Thien-Tanner Fluid through asymmetric channel." *Korea-Australia Rheology Journal* 32, no. 4 (2020): 271-285. https://doi.org/10.1007/s13367-020-0026-1
[19] Saleem, Anber, Salman Akhtar, and Sohail Nadeem. "Bio-mathematical analysis of electro-osmotically modulated hemodynamic blood flow inside a symmetric and nonsymmetric stenosed artery with joule heating." *International Journal of Biomathematics* 15, no. 02 (2022): 2150071. https://doi.org/10.1142/S1793524521500716
[20] Khan, Ambreen Afsar, Kaenat Akram, Akbar Zaman, O. Anwar Bég, and Tasveer Anwar Bég. "Electro-osmotic peristaltic flow and heat transfer in an ionic viscoelastic fluid through a curved micro-channel with viscous dissipation." *Proceedings of the Institution of Mechanical Engineers, Part H: Journal of Engineering in Medicine* 236, no. 8 (2022): 1080-1092. https://doi.org/10.1177/09544119221105848
[21] Butt, Adil Wahid, Noreen Sher Akbar, Rashid Mehmood, and Shahid Farooq. "Thermally conductive electro-osmotic propulsive pressure-driven peristaltic streaming flow study with a suspended nanomaterial in a micro-ciliated tube." *Frontiers in Materials* 9 (2022): 1059816. https://doi.org/10.3389/fmats.2022.1059816
[22] Sadaf, Hina, and Sohail Nadeem. "Analysis of combined convective and viscous dissipation effects for peristaltic flow of Rabinowitsch fluid model." *Journal of Bionic Engineering* 14, no. 1 (2017): 182-190. https://doi.org/10.1016/S1672-6529(16)60389-X
[23] Vaidya, Hanumesh, C. Rajashekhar, G. Manjunatha, K. V. Prasad, O. D. Makinde, and K. Vajravelu. "Heat and mass transfer analysis of MHD peristaltic flow through a complaint porous channel with variable thermal conductivity." *Physica Scripta* 95, no. 4 (2020): 045219. https://doi.org/10.1088/1402-4896/ab681a
[24] Abd-Alla, A. M., S. M. Abo-Dahab, Esraa N. Thabet, and M. A. Abdelhafez. "Heat and mass transfer for MHD peristaltic flow in a micropolar nanofluid: mathematical model with thermophysical features." *Scientific Reports* 12, no. 1 (2022): 21540. https://doi.org/10.1038/s41598-022-26057-6
[25] Eldabe, Nabil Tawfik, Mohamed Abouzeid, and Hamida A. Shawky. "MHD peristaltic transport of Bingham blood

fluid with heat and mass transfer through a non-uniform channel." *Journal of Advanced Research in Fluid Mechanics and Thermal Sciences* 77, no. 2 (2021): 145-159. https://doi.org/10.37934/arfmts.77.2.145159

[26] Abo-Dahab, Sayed M., Ramadan A. Mohamed, Abdelmoaty M. Abd-Alla, and Mahmoud S. Soliman. "Double-diffusive peristaltic MHD Sisko nanofluid flow through a porous medium in presence of non-linear thermal radiation, heat generation/absorption, and Joule heating." *Scientific Reports* 13, no. 1 (2023): 1432. https://doi.org/10.1038/s41598-023-27818-7

[27] Channakote, Mahadev M., and Dilipkumar V. Kalse. "Heat Transfer in Peristaltic Motion of Rabinowitsch Fluid in a Channel with Permeable wall." *Applications & Applied Mathematics* 16, no. 2 (2021).

[28] Beleri, Joonabi, and Asha S. Kotnurkar. "Peristaltic Transport of Ellis Fluid under the Influence of Viscous Dissipation Through a Non-Uniform Channel by Multi-Step Differential Transformation Method." *Journal of Advanced Research in Numerical Heat Transfer* 9, no. 1 (2022): 1-18.

[29] Channakote, Mahadev M., and D. V. Kalse. "Combined convective and viscous dissipation effects on peristaltic flow of ellis fluid in a non-uniform tube." *Journal of Naval Architecture & Marine Engineering* 19, no. 1 (2022). https://doi.org/10.3329/jname.v19i1.55052

[30] Sinha, A., and G. C. Shit. "Electromagnetohydrodynamic flow of blood and heat transfer in a capillary with thermal radiation." *Journal of Magnetism and Magnetic Materials* 378 (2015): 143-151. https://doi.org/10.1016/j.jmmm.2014.11.029

[31] Shit, G. C., A. Mondal, A. Sinha, and P. K. Kundu. "Electro-osmotically driven MHD flow and heat transfer in micro-channel." *Physica A: Statistical Mechanics and Its Applications* 449 (2016): 437-454. https://doi.org/10.1016/j.physa.2016.01.008

[32] Hasen, Saba S., and Ahmed M. Abdulhadi. "Analytical Study of Soret and Dufour effect in the Electro-osmotic peristaltic flow of Rabinowitsch fluid model." *Ibn Al-Haitham Journal for Pure and Applied Sciences* 34, no. 2 (2021): 70-86. https://doi.org/10.30526/34.2.2629

[33] Noreen, S., Quratulain Quratulain, and D. Tripathi. "Heat transfer analysis on electroosmotic flow via peristaltic pumping in non-Darcy porous medium." *Thermal Science and Engineering Progress* 11 (2019): 254-262. https://doi.org/10.1016/j.tsep.2019.03.015

[34] Guo, Xiaoyi, and Haitao Qi. "Analytical solution of electro-osmotic peristalsis of fractional Jeffreys fluid in a micro-channel." *Micromachines* 8, no. 12 (2017): 341. https://doi.org/10.3390/mi8120341

[35] Channakote, Mahadev M., and S. K. Asha. "Heat transfer and electro-osmotic analysis on peristaltic pumping of a fractional second-grade fluid through a cylindrical tube." *International Journal of Computational Materials Science and Engineering* 12, no. 04 (2023): 2350007. https://doi.org/10.1142/S2047684123500070

[36] Tripathi, Dharmendra. "Peristaltic flow of a fractional second grade fluid through a cylindrical tube." *Thermal Science* 15, no. suppl. 2 (2011): 167-173. https://doi.org/10.2298/TSCI100503061T

[37] Abd-Alla, A. M., S. M. Abo-Dahab, Esraa N. Thabet, and M. A. Abdelhafez. "Peristaltic pump with heat and mass transfer of a fractional second grade fluid through porous medium inside a tube." *Scientific Reports* 12, no. 1 (2022): 10608. https://doi.org/10.1038/s41598-022-14773-y

[38] Hameed, M., Ambreen A. Khan, R. Ellahi, and M. Raza. "Study of magnetic and heat transfer on the peristaltic transport of a fractional second grade fluid in a vertical tube." *Engineering Science and Technology, an International Journal* 18, no. 3 (2015): 496-502. https://doi.org/10.1016/j.jestch.2015.03.004

[39] Rathod, Vijaykumar P., and M. Mahadev. "Interaction of heat transfer and peristaltic pumping of fractional second grade fluid through a vertical cylindrcal tube." *Thermal Science* 18, no. 4 (2014): 1109-1118. https://doi.org/10.2298/TSCI111022143R

[40] Hu, Yang, Decai Li, Xiaodong Niu, and Yanjuan Zhang. "Lattice Boltzmann model for the axisymmetric electro-thermo-convection." *Computers & Mathematics with Applications* 78, no. 1 (2019): 55-65. https://doi.org/10.1016/j.camwa.2019.02.006

[41] Hu, Yang, Decai Li, Xiaodong Niu, and Shi Shu. "An immersed boundary-lattice Boltzmann method for electro-thermo-convection in complex geometries." *International Journal of Thermal Sciences* 140 (2019): 280-297. https://doi.org/10.1016/j.ijthermalsci.2019.02.015